A Possible Mechanism for the Eye Rotation of Typhoon Herb

HUNG-CHI KUO

Department of Atmospheric Science, National Taiwan University, Taipei, Taiwan

R. T. WILLIAMS

Department of Meteorology, Naval Postgraduate School, Monterey, California

JEN-HER CHEN

Central Weather Bureau, Taipei, Taiwan

(Manuscript received 9 January 1998, in final form 20 July 1998)

ABSTRACT

An elliptical eye that rotated cyclonically with a period of approximately 144 minutes in Typhoon Herb 1996 was documented. The elliptical region had a semimajor axis of 30 km and a semiminor axis of 20 km. Two complete periods of approximately 144 min were observed in the Doppler radar data. The rotation of the elliptical eye in the context of barotropic dynamics at three levels were explored: linear waves on a Rankin vortex, a nonlinear Kirchhoff vortex, and with a nonlinear spectral model. The linear wave theory involves the existence of both the high (potential) vorticity gradient near the eye edge and the cyclonic mean tangential flow in the typhoon. The propagation of (potential) vorticity waves in the cyclonic mean flow makes the elliptical eye rotate cyclonically. The rotation period is longer than the period of a parcel trajectory moving in the cyclonic mean flow around the circumference, because the vorticity wave propagates upwind. The nonlinear theory stems from the rotation of Kirchhoff's vortex. Estimates of the eye rotation period from both linear and nonlinear theories agree with observations of the eye rotation period when the observed maximum wind from Herb is used. Nonlinear numerical computations suggest the importance of the interaction of neutral vorticity waves, which determine the shape and the rotation period of the eye. The calculations also support the rotation of the eye in approximately 144 min in the presence of axisymmetrization, vorticity redistribution, wave breaking, and vortex merging processes.

1. Introduction

The eyewall of a typhoon is often circular in shape. However, using photographic records of storms observed with both land-based and airborne radars, Lewis and Hawkins (1982) documented cyclonically rotating polygonal eyewalls. A wide variety of shapes was observed, including triangles, squares, pentagons, hexagons, and incomplete versions of many polygons. Circular and elliptical shapes were also noted in their review, but such smooth shapes were often quickly replaced by polygonal features. Because they found polygonal eyewalls using airborne 5-cm radars far offshore, Lewis and Hawkins concluded that proximity to land is not a requirement for the generation of polygonal features. Lewis and Hawkins concluded that polygonal eyewalls could be attributed to the partial reflection of inward propagating gravity waves with different wavenumber and periods, an idea whose origin is in the theoretical work of Kurihara (1976) and Willoughby (1978). Unfortunately, the period of rotation of the polygonal features was not examined in the Lewis and Hawkins study.

Using a remarkable 15-h record from land-based radar, Muramatsu (1986) also observed polygonal eyewalls in Typhoon Wynne 1980. The polygonal features consisted of cyclonically rotating squares, pentagons, and hexagons. The pentagons and hexagons had rotational periods of approximately 42 min, and the squares had periods of approximately 48 min. This decrease in the rotational period with increasing tangential wavenumber will be discussed further in the theoretical argument presented here.

Typhoon Herb in 1996 was the strongest typhoon to hit Taiwan in the last decade. Based on wind observations 700 m above mean sea level on Wu-Feng Mountain, the maximum wind in Herb was estimated to be

Corresponding author address: Dr. R. T. Williams, Department of Meteorology, NPS/MR/Wu/jn, Naval Postgraduate School, Monterey, CA 93943.
E-mail: williart@met.nps.navy.mil

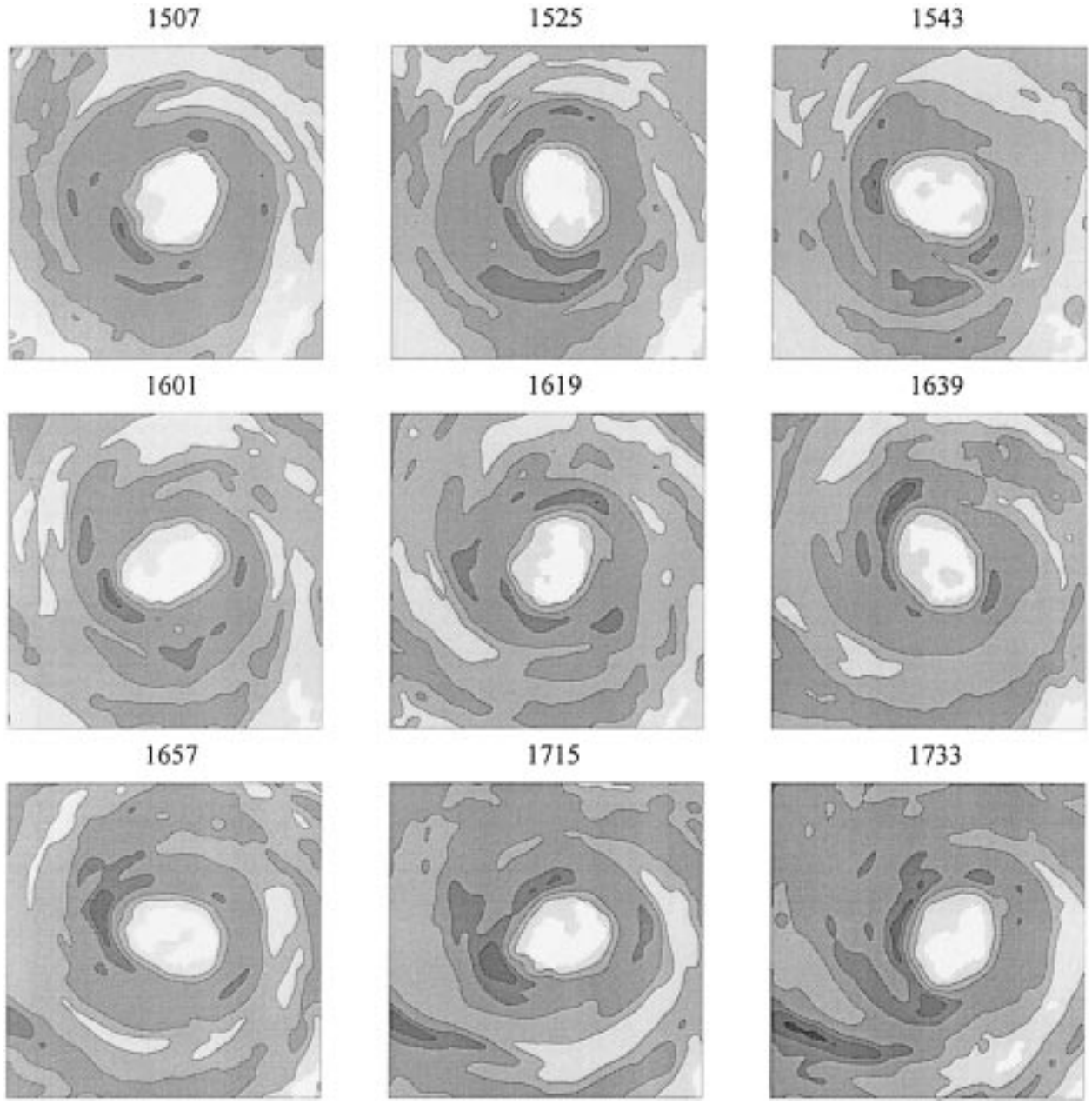

FIG. 1. Horizontal distribution of maximum reflectivity in the vertical column for Typhoon Herb from the Central Weather Bureau WSR-88D (10 cm) radar at Wu-Feng Mountain on 31 Jul 1996. The sequence of images is from left to right and from top to bottom. The time interval between each image is approximately 18 min. The local time of observation is indicated on top of each image. The major axis radius in the eye region is about 30 km and the minor axis radius is about 20 km. The nine images illustrate one eye rotation period of 144 min.

60 m s^{-1} or higher [see also Lee (1997) for Doppler winds analysis]. It destroyed the newly installed Central Weather Bureau WSR-88D Doppler radar on Wu-Feng Mountain. Before the destruction of the radar, the radar pictures revealed that Herb had an elliptical eye that rotated cyclonically with a period of approximately 144 min. Two complete periods were observed. The objective of this paper is to document the elliptical eye rotation and to explore possible mechanisms for the eye rotation. Section 2 gives the radar observations and theories for the eye rotation. Numerical results are presented in section 3, and concluding remarks are in section 4.

2. Observations and theories

Figures 1 and 2 are the radar pictures of Typhoon Herb from the Central Weather Bureau WSR-88D

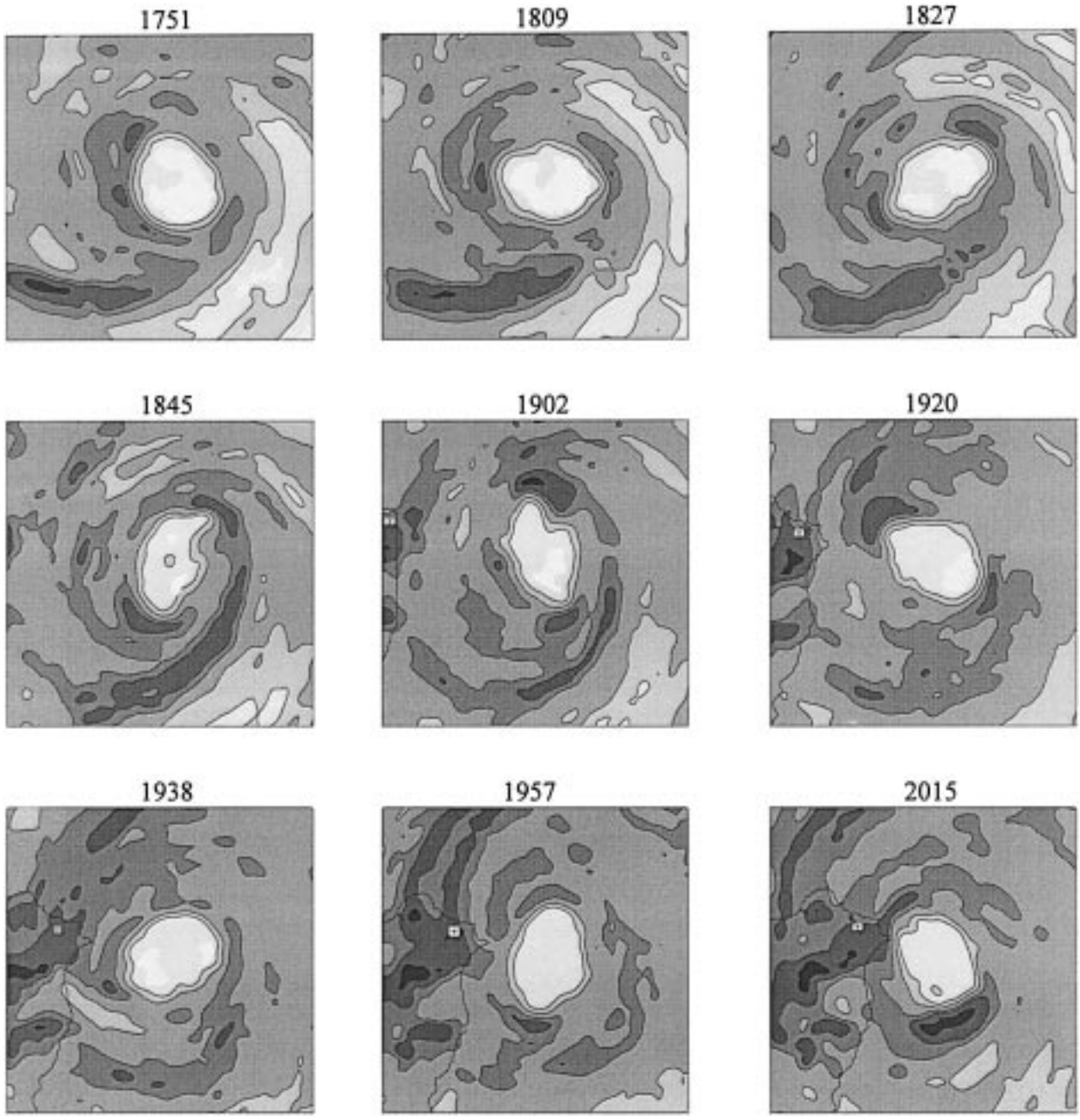

FIG. 2. Similar to Fig. 1 except for the second rotation period. In this observation period Typhoon Herb is closer to the radar.

Doppler radar. The sequence of the pictures in each figure is from left to right and from top to bottom, and the time interval between each image is approximately 18 min. Each of the two sets of images in Figs. 1 and 2 illustrate one complete cyclonic eye rotation with a period of 144 min. Thus, there are two complete periods of approximately 144 min in the elliptical eye rotation that have been observed with the radar. Since the radar pictures in Figs. 1 and 2 represent the maximum reflectivity in each vertical column, the elliptical eye is a deep tropospheric phenomenon. Other PPI images (not shown here) indicate that the elliptical eye is the most dominate feature at each vertical level. Significant polygonal features were not observed on any individual level, although some irregular eyes in the images were noticed in the second rotation period. In this observation period, Typhoon Herb is closer to Taiwan. The elliptical region observed in the figures has a semimajor axis of 30 km and a semiminor axis of 20 km, approximately.

It is interesting to note that there was often deep convection (strong reflectivity regions) near the tips of the major axis in the elliptical eye.

The timescale for a parcel circulating around the circumference of the eye region, based on the observed maximum wind of 60 m s^{-1} and on the size of the major axis and minor axis, was approximately 50 min. The elliptical eye rotation period of 144 min is much longer than the parcel circuit time. The existence of an elliptical eye with a long period of rotation (144 min) in Typhoon Herb seems to be a unique feature that has not been found in previous studies.[1] An important question is, what mechanism caused the elliptical eye to rotate more slowly than the period related to the maximum wind speed?

We consider the elliptical eye shape as a wavenumber 2 asymmetry of a circular eye. The eye is viewed as a region of nearly constant and high (potential) vorticity with a large (potential) vorticity gradient at its edge. Under the conservation of (potential) vorticity, the gradient of (potential) vorticity provides a state on which (potential) vorticity waves (the generalization of Rossby waves) can propagate. Thus, the wavenumber 2 asymmetries near the eye edge should propagate to the left of the vorticity gradient, which means that the asymmetries should move upstream with respect to the mean flow. This effect would cause the elliptical eye to rotate anticyclonically with respect to the mean wind. However, with the strong cyclonic tangential mean flow in the typhoon, the wave asymmetries should propagate downstream, but with a propagation speed slower than the advective speed. This wavenumber 2 asymmetry propagation corresponds to a cyclonic elliptical eye rotation. The linear analysis of the (potential) vorticity wave on a Rankine vortex was done by Sir William Thomson (Lord Kelvin) in 1880 (Thomson 1880) and was summarized by Lamb (1932) and by Guinn and Schubert (1993). His analysis indicates that the speed of the wave is given by

$$c = V_{\max}\left(1 - \frac{1}{m}\right), \tag{2.1a}$$

with $V_{\max}$ the maximum tangential speed of the cyclonic mean flow and m the tangential wavenumber. Equation (2.1a) indicates that wavenumber 1 is stationary and wavenumbers $m = 2$, 3, and 4 move, respectively, at ½, ⅔, and ¾ the speed of the basic-state tangential flow. For the elliptical eye we take the m to be 2. The angular velocity is then $\omega_a = c/r = V_{\max}/2r$ and the rotation period is

$$P = \frac{2\pi}{\omega_a} = \frac{8\pi}{\zeta}, \tag{2.1b}$$

where $\zeta = 2V_{\max}/r$ is the vorticity inside the eye region. When the period of 144 min is considered, the vorticity strength from (2.1b) is about 3×10^{-3} s^{-1}. With the size of Typhoon Herb, the 3×10^{-3} s^{-1} vorticity field corresponds to a maximum wind speed of 60 m s^{-1}. This is in agreement with the maximum wind observed in Typhoon Herb.

The wavenumber m for polygonal eyes would be greater than 2. In this case the linear theory [(2.1a)] predicts a phase speed that is closer to $V_{\max}$, which corresponds to a shorter period. This agrees qualitatively with the period of Typhoon Herb and the period observed by Muramatsu (1986). The decrease in rotation period as the number of sides of polygon increased is also consistent with the linear theory. More detailed comparisons with theory cannot be made because Muramatsu (1986) did not give such key information as the maximum wind speed in the eyewall region.

The rotation of elliptical eye can also be interpreted as a wavenumber 1 feature rotating about one focus. However, the wavenumber 1 feature in this case is more of finite amplitude in nature. The linear theory may not be well applied. To avoid the arbitrariness in the interpretation, we now consider a more general nonlinear dynamical theory for the elliptical eye rotation. Consider an elliptical shaped vortex patch, that is, an ellipse,

$$\frac{x^2}{a^2} + \frac{y^2}{b^2} = 1, \tag{2.2}$$

with semimajor axis a and semiminor axis b, inside of which the vorticity has the constant value ζ and outside of which the vorticity vanishes. This is the so-called Kirchhoff elliptical vortex. It was shown by Kirchhoff (Lamb 1932, p. 232) that this elliptical vortex region will rotate, without change of shape, at the angular velocity

$$\omega_a = \zeta\frac{ab}{(a + b)^2}. \tag{2.3}$$

The rotation period of the Kirchhoff vortex is

$$P = \frac{2\pi}{\omega_a} = \frac{2\pi}{\zeta}\frac{(a + b)^2}{ab}. \tag{2.4}$$

In the limit of a vortex with small eccentricity, (2.4) yields the same result as the linear case of (2.1b). It can be shown that (2.4) differs from (2.1b) by $O(\epsilon^2)$ where $\epsilon = (a - b)/a$. Namely, an ϵ of 50% will result in a 12.5% difference between (2.4) and (2.1b). With the semimajor axis of 30 km and semiminor axis of 20 km as in Typhoon Herb, we obtain

[1] Kurihara and Bender (1982) found in their 5-km resolution modeling study of tropical cyclones that asymmetry in the vortex structure is evident in various fields. Regions of anomalous rainfall intensity, temperature anomaly, and ascending motion are simulated at a few locations within the eyewall. The asymmetric features within the eyewall moved cyclonically at a much smaller rotation rate than the cyclonic wind within the eyewall. Attention in the paper is given to the balance between the wind and pressure fields and to the budgets of angular momentum, heat, and water vapor.

$$P = \frac{2\pi}{\zeta}\frac{25}{6} \approx \frac{8\pi}{\zeta}. \tag{2.5}$$

Thus, both the linear theory of vorticity waves and the nonlinear theory of the Kirchhoff elliptical vortex give virtually the same result. The theories agree well with the observed rotation period based on the size of the eye region and the maximum wind speed in Typhoon Herb. The Rankine vortex structure is assumed in the above theories. There were no aircraft observations for Typhoon Herb. The only observations were made by the WSR-88D radar. Unfortunately the detailed structure of (potential) vorticity inside the eye region is not available from the very limited observations (Lee 1997).

3. Numerical results

Moist convective processes near the tropical cyclone center continuously conspire to make high (potential) vorticity in the eyewall. The vorticity field is continuously modified by axisymmetrization (or by the damping of asymmetric kinetic energy), vorticity wave breaking, and vortex merging. Carr and Williams (1989) used a nondivergent, barotropic model to identify the asymmetry-damping influence of symmetric angular wind shear outside the radius of maximum wind as the mechanism by which a barotropic vortex resists asymmetric forcing. To substantiate the theories of the eye rotation in the presence of axisymmetrization or vortex stablization processes, we perform nonlinear calculations with a nondivergent barotropic model on the f plane. The discretization of the barotropic model is based on the Fourier–Chebyshev spectral method in space and the fourth-order Runge–Kutta method in time (Fulton and Schubert 1987; Kuo and Schubert 1988). The computational domain is a square region that is 216 × 216 km. We employ 216 collocation points in each direction. The wave truncation in the spectral domain ensures the elimination of aliasing error in the quadratic nonlinear terms. No numerical diffusion is employed in the time integration.

We consider the following structure functions for our numerical experiments. The first function gives a vorticity profile that resembles the Rankine vortex

$$P(r) = \begin{cases} \left\{1 - \exp\left[-\dfrac{30}{r}\exp\left(\dfrac{1}{r-1}\right)\right]\right\}, & \text{if } r < 1; \\ 0, & \text{otherwise,} \end{cases} \tag{3.1a}$$

where r is a nondimensional distance. The second is the Gaussian function

$$G(r) = \exp(-r^2). \tag{3.1b}$$

The $P(r)$ is an analytical approximation to the step function. The $P(r)$ is introduced to avoid to occurrence of the Gibbs phenomenon in the spectral model.

Our first experiment (expt. 1) involves an elliptical Rankine-like vortex with a 0.003 s^{-1} vorticity field and with the scale of Typhoon Herb. The Rankine-like vortex is specified according to

$$\zeta(r) = \zeta_0 P(r), \tag{3.2}$$

$$r = \left[\left(\frac{x - x_0}{a}\right)^2 + \left(\frac{y - y_0}{b}\right)^2\right]^{1/2}, \tag{3.3}$$

where x_0 and y_0 are the center of the eye, $a = 30$ km, $b = 20$ km, and $\zeta_0 = 0.003$ s^{-1}.

Figure 3a gives the initial vorticity profiles in the semimajor axis direction for experiment 1 (the vorticity unit is 10^{-3} s^{-1}). The vorticity distribution according to (3.1a) and (3.2) resembles the shape of a plateau. The 0.003 s^{-1} vorticity field approximately corresponds to a maximum wind of 60 m s^{-1}. The vorticity field outside the elliptical vortex is zero in this experiment. Figure 4 gives the vorticity field for experiment 1 at 0 and 144 min. Only the interior square region 100 × 100 km in the computational domain is shown. Moreover, thin filaments of vorticity outside the ellipse are not contoured in the figure for clarity. The eye remains an ellipse despite the presence of the wave-breaking process. Figure 4 shows that the elliptical eye as represented by a Rankine-like vortex with a 0.003 s^{-1} vorticity field rotates cyclonically with a period of 144 min without changing shape. This is in agreement with both the observations and our simple theories for the eye rotation in Typhoon Herb. Figure 4 also demonstrates the accuracy of the numerical model with a nearly discontinuous initial vorticity field because the Kirchhoff vortex is an exact solution of the vorticity equation.

Maintenance of elliptical shape is expected according to Carr and Williams (1989). By introducing cylindrical coordinates and decomposing the physical field into symmetric and asymmetric components, it can be shown that the area-averaged asymmetric kinetic energy E_a in an annular region between radii r_a and r_b can be expressed as

$$\frac{\partial E_a}{\partial t} = -\int_{r_a}^{r_b} \overline{v_a u_a}\frac{\partial \omega_s}{\partial r} r^2\, dr, \tag{3.4}$$

where $\overline{(\,)}$ is the tangential average, $\omega_s = v_s/r$ the symmetric angular wind, v_s the symmetric tangential wind, u_a the asymmetric radial velocity, and v_a the asymmetric tangential velocity. For a Rankine vortex, ω_s is equal to a constant and there can only be neutral waves without damping according to (3.4). Thus, the vortex rotates without changing its shape. A more complete analysis that includes the full domain was carried out by Smith and Montgomery (1995).

Our second experiment (expt. 2) involves an elliptical vortex with a Gaussian vorticity distribution

$$\zeta(r) = \zeta_0 G(r), \tag{3.5}$$

where r is defined in (3.3). The peak vorticity at the center of the eye is taken to be 0.005 s^{-1}. The initial

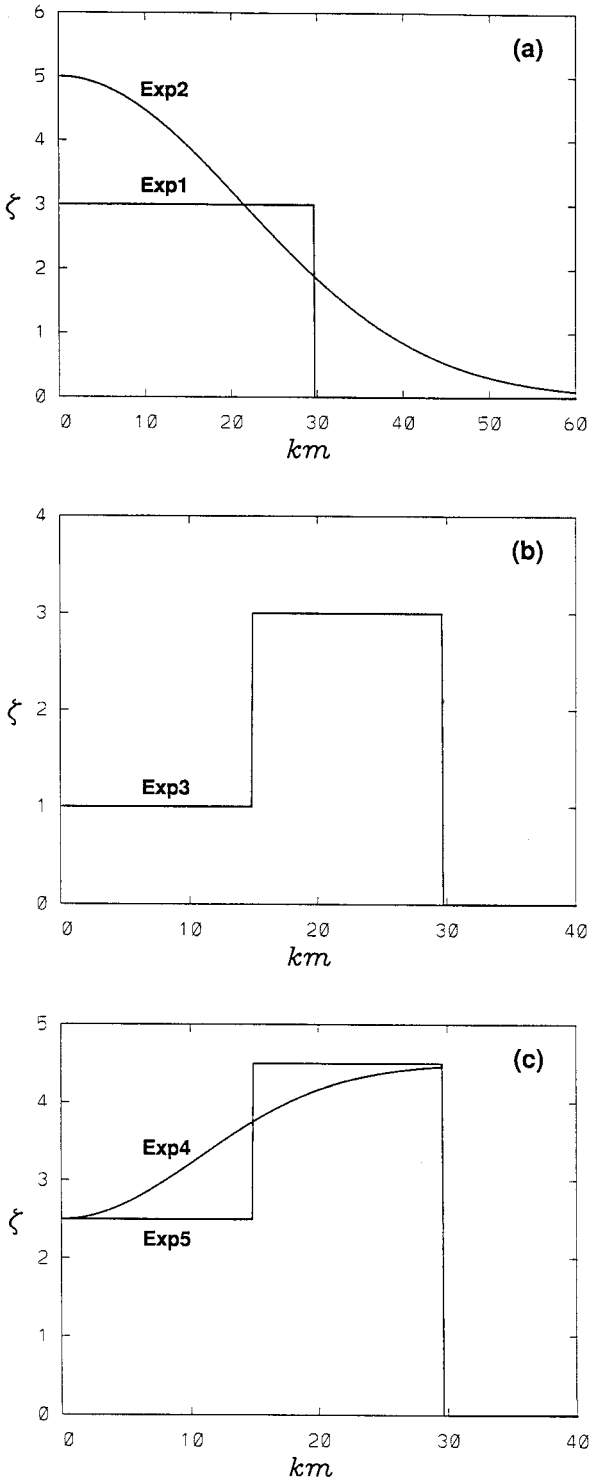

FIG. 3. The initial vorticity profiles in the semimajor axis direction for (a) expt. 1 and expt. 2, (b) expt. 3, and (c) expt. 4 and expt. 5. The unit on the ordinate is 10^{-3} s^{-1}.

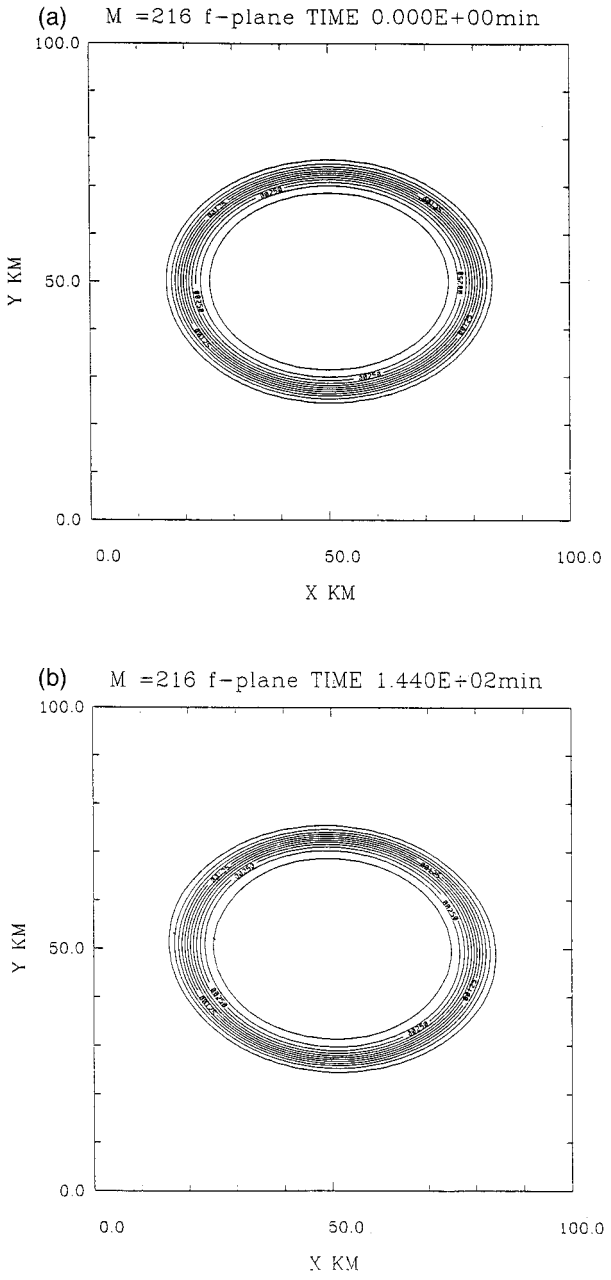

FIG. 4. The vorticity field for expt. 1 at 0 and 144 min. A square region 100 × 100 km in the computational domain is shown. The contour interval is 0.00025 s^{-1}.

semimajor axis vorticity profile can also be seen in Fig. 3a. The design of the experiment does not imply that the vorticity distribution in the eye region resembles the Gaussian function, but rather it is designed to show that the maintenance of the elliptical eye is crucially dependent on the vorticity distribution in the eye region. The vorticity distribution sets the dynamic background for the presence of neutral waves and/or asymmetry-damp-

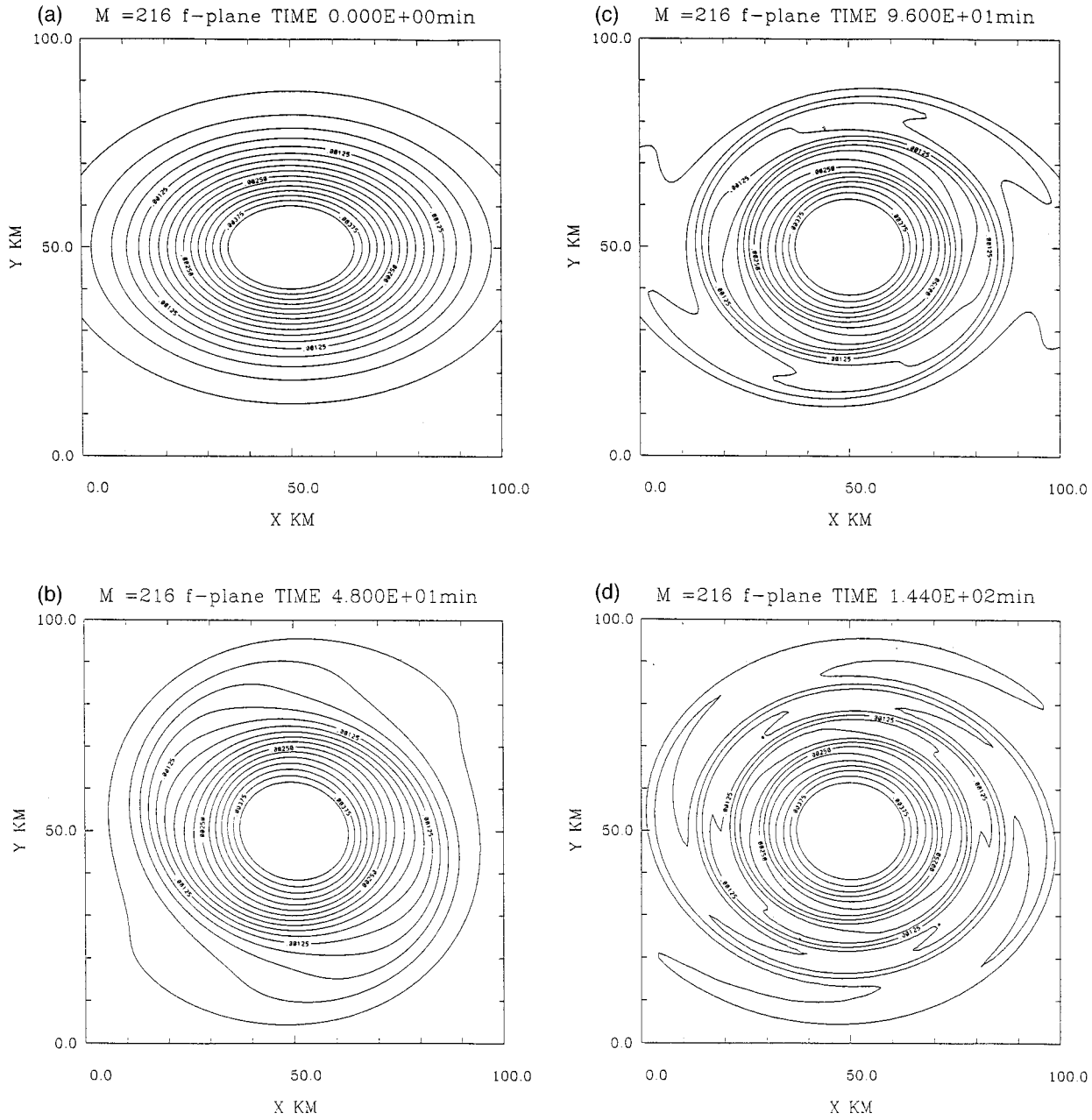

FIG. 5. The vorticity field for expt. 2 at 0, 48, 96, and 144 min. A square region 100 × 100 km in the computational domain is shown. The contour interval is 0.00025 s^{-1}.

ing processes. With the Gaussian structure as in (3.5), $\partial\omega_s/\partial r$ is not zero, so a disturbance can either grow or decay depending on the tilt of the waves. Figure 5 gives the initial vortex and the numerical results in 48-min intervals up to 144 min. It is clear from Fig. 5 that axisymmetrization or vortex stablization processes (Melander et al. 1987; Carr and Williams 1989) have produced a nearly circular vortex with surrounding filaments of vorticity. Details of the axisymmetrization as they relate to hurricane dynamics were discussed by Carr and Williams (1989), Guinn and Schubert (1993), Smith and Montgomery (1995), Montgomery and Kallenbach (1997), and Montgomery and Enagonio (1998). Due to the asymmetry damping, it is difficult to identify any distinct rotation period in this experiment. These two experiments suggest that the maintenance of an elliptical vortex is dependent on the vortex structure. This is consistent with the finding of Dritschel (1998) that the steepness of the vortex edge controls the vortex axisymmetrization.

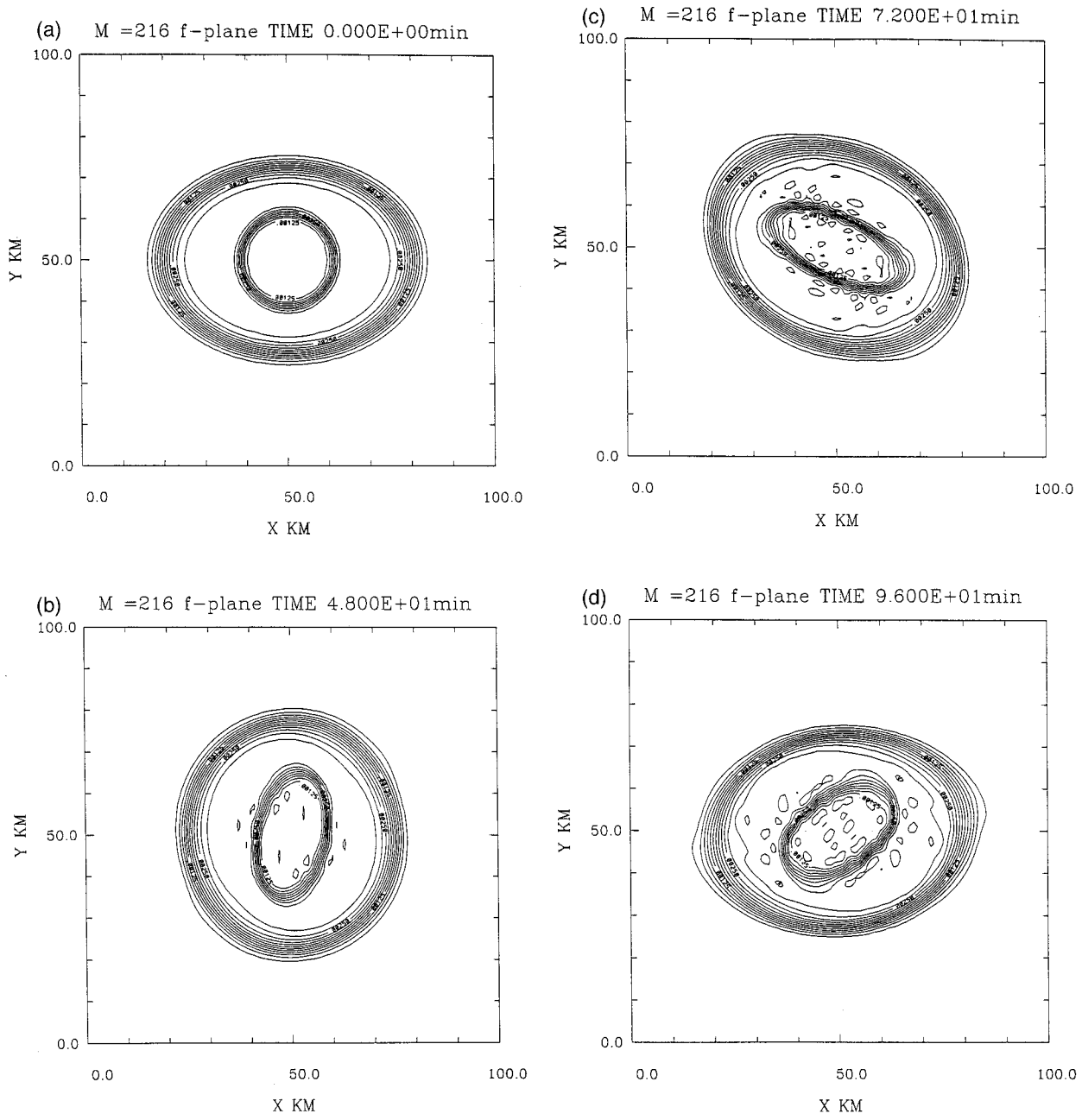

FIG. 6. The vorticity field for expt. 3 at 0, 48, 72, 96, 120, and 144 min. A square region 100 × 100 km in the computational domain is shown. The contour interval is 0.00025 s^{-1}.

Our third experiment (expt. 3) is with the initial condition

$$\zeta(r) = \zeta_0 P(r) - \Delta\zeta P(r_*), \tag{3.6}$$

$$r_* = \left[\left(\frac{x - x_0}{a_*}\right)^2 + \left(\frac{y - y_0}{b_*}\right)^2\right]^{1/2}, \tag{3.7}$$

where $a_* = 15$ km, $b_* = 15$ km, $\zeta_0 = 0.003$ s^{-1}, and $\Delta\zeta = 0.002$ s^{-1}, and r is computed according to (3.3). The design of this experiment stems from the idea that there is no significant latent heat release in the central region of the eye. A slightly lower value of potential vorticity may be expected prior to any potential vorticity lateral mixing or redistribution. The vorticity profile in the semimajor axis direction is given in Fig. 3b. This profile gives an outer elliptic region of 0.003 s^{-1} vorticity with an inner circular region of 0.001 s^{-1} vorticity

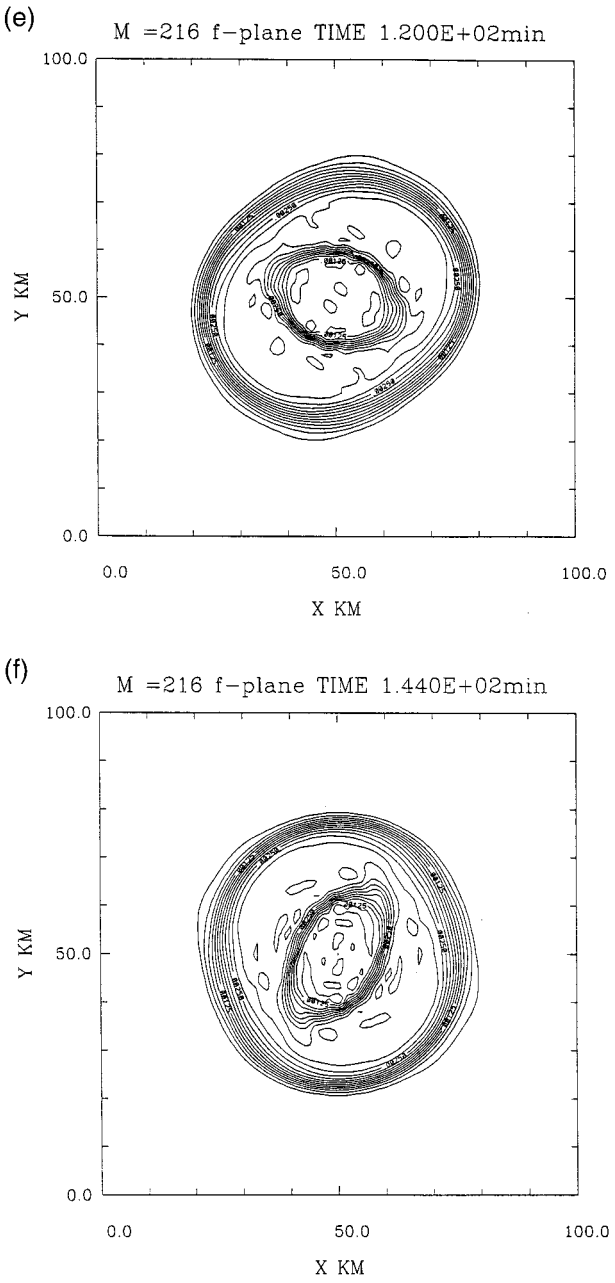

FIG. 6. (*Continued*)

and a region of zero vorticity on the outside. With the Rankine-like vortex structure inside the eye, the purpose of experiment 3 is to investigate the impact on the eye rotation of the interaction of neutral vorticity waves.

Figure 6 gives the vorticity field for experiment 3 at 0, 48, 72, 96, 120, and 144 min. It is obvious from Fig. 6 that the elliptical vortex does not rotate in 144 min. Figure 6 indicates that there are neutral vorticity waves that appear on both sides of the annular region of vorticity. Analysis in the appendix suggests that wavenumbers 1 and 2 are always stable despite the fact that the necessary condition of barotropic instability is satisfied. In addition, wavenumber 4 is stable with our experiment parameters. The analysis in the appendix suggests that the inner and outer vorticity waves should move out of phase, with the inner waves moving more rapidly. The figures show that wavenumber 4 is moving out of phase with wavenumber 2, which leads to the formation of a box-shaped vortex. It appears that waves 2 and 4 move out of phase because the nonlinear effects can no longer hold them together. This occurs because nonlinear solutions cannot be superposed. On the other hand, in experiment 1 and in the Kirchhoff solution, wavenumber 4 is locked with wavenumber 2 and all of the higher wavenumbers. The Kirchhoff solution with the parameters from experiment 1 is already in the nonlinear range. It is the nonlinear effects that keep all waves moving in phase at the same phase speed. If all of the waves moved linearly they would move out of phase. Figures 4, 5, and 6 suggest that maintenance of the elliptical-shaped vortex as well as the rotation period are very sensitive to the vorticity structure inside the eye region.

Our fourth experiment (expt. 4) is with the initial condition

$$\zeta(r) = \zeta_0 P(r) - \Delta\zeta G(r_*), \tag{3.8}$$

where $\zeta_0 = 0.0045\ \text{s}^{-1}$, $\Delta\zeta = 0.002\ \text{s}^{-1}$, $a = 30$ km, $b = 20$ km, $a_* = 15$ km, and $b_* = 10$ km. Equation (3.8) gives a vorticity field at the center of the elliptical eye of $0.0025\ \text{s}^{-1}$ and the vorticity field increases to $0.0045\ \text{s}^{-1}$ near the vortex edge. The size of the eye is about the same as in Typhoon Herb. The semimajor axis profile of vorticity is shown in Fig. 3c. Figure 7 gives the vorticity field for experiment 4 at 0, 48, 96, and 144 min. Two filaments of vorticity outside the ellipse are present at the end of integration. The eye remains an ellipse and rotates cyclonically with a period of 144 min despite the presence of the minimum vorticity structure.

Our fifth experiment (expt. 5) is with the initial condition

$$\zeta(r) = \zeta_0 P(r) - \Delta\zeta P(r_*) \tag{3.9}$$

where $\zeta_0 = 0.0045\ \text{s}^{-1}$, $\Delta\zeta = 0.002\ \text{s}^{-1}$, $a = 30$ km, $b = 20$ km, $a_* = 15$ km, and $b_* = 10$ km. The only difference between experiments 5 and 4 is the interior vorticity structure. The semimajor axis profile of vorticity is shown in Fig. 3c. Figure 8 gives the vorticity field for experiment 5 at 96 and 144 min. It is clear that a box-shaped outer vortex forms due to the interaction of neutral vorticity waves. The outer vortex does not rotate with a period of 144 min.

Our last two experiments, experiments 6 and 7, are the same as experiments 4 and 5, respectively, except that an asymmetric vorticity field of the order $0.0015\ \text{s}^{-1}$ in the east quadrants of the elliptical-shaped vortex is added. Furthermore, we have modified our ζ_0 value from 0.0045 to $0.005\ \text{s}^{-1}$ in experiments 6 and 7. The asymmetric vorticity outside the eye may be viewed as

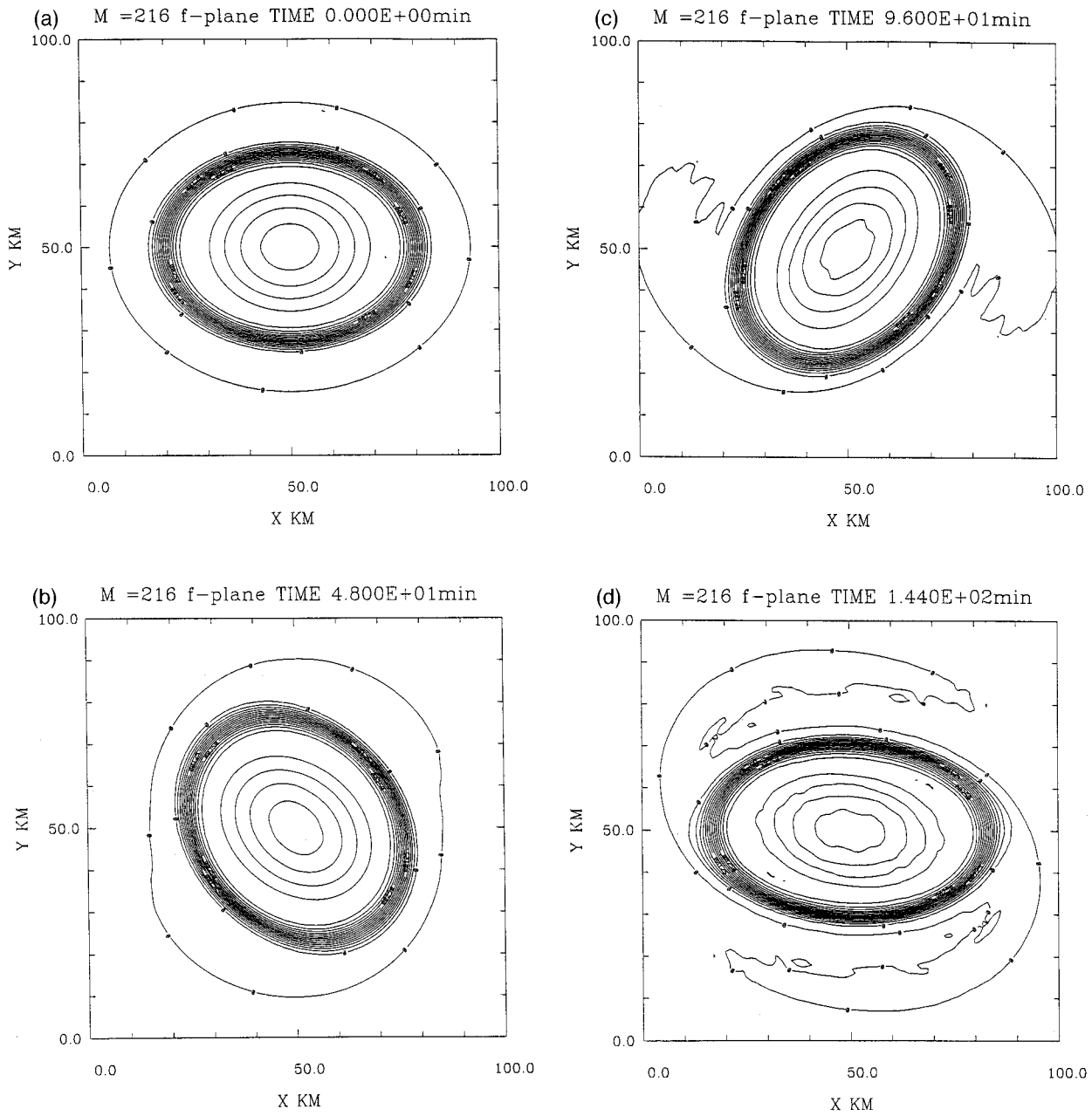

FIG. 7. The vorticity field for expt. 4 at 0, 48, 96 and 144 minutes. A square region 100 × 100 km in the computational domain is shown. The contour interval is 0.00025 s^{-1}.

coming from some random convection outside the eye. Figure 9 gives the vorticity field for experiment 6 at 0, 48, 96, and 144 min. A region 150 × 150 km in the computational domain is shown. Figure 9 indicates that the neighboring vorticity is quickly elongated and wrapped around the elliptical eye. There are also wave-breaking and vorticity redistribution processes (e.g., Schubert et al. 1997; Schubert et al. 1999) associated with the elliptical vortex. The center of the elliptical eye translates a distance of 30 km toward the northwest. The eye continues to be an ellipse throughout the integration. The elliptical eye also rotates with a period of 144 min in the presence of vorticity redistribution, vortex translation, vortex merging, and wave-breaking processes. Figure 10 gives the vorticity field for experiment 7 at 96 and 144 min. We observe the vortex has been distorted significantly from the elliptical shape and the rotation period is very difficult to determine.

Some of our model integrations reproduce the cyclonic rotation of the elliptical eye with a period of approximately 144 min. The maintenance of an elliptical-shaped vortex requires a vortcity structure that re-

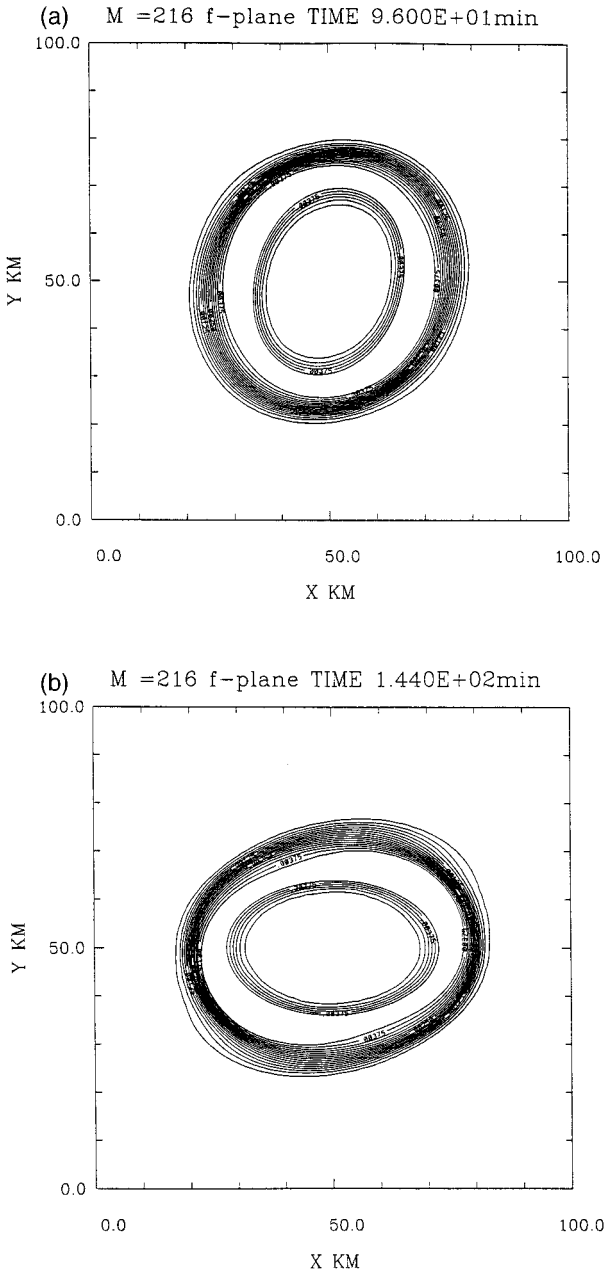

FIG. 8. Similar to Fig. 7 except for expt. 5 at 96 and 144 min.

sembles the Rankine vortex. The rotation period is sensitive to the peak vorticity value. When a minimum vorticity in the center of the eye is considered, the rotation period as well as the maintenance of elliptical shape are crucially dependent on the spatial structure of the minimum vorticity region. The interaction of neutral vorticity waves plays an important role in determining the shape and the rotation period of the eye. A minimum vorticity region inside the eye with the structure given by (3.1a) often distorts the shape and changes the rotation period of the elliptical eye. This is in agreement with the analysis in section 2 and in the appendix.

4. Summary and concluding remarks

We have documented an elliptical eye that rotated cyclonically with a period of approximately 144 min in Typhoon Herb. The elliptical region had a major axis radius of 30 km and a minor axis radius of 20 km. Two complete periods of approximately 144 min each were observed with the Doppler radar. We propose two theories to explain the eye rotation. The linear wave theory requires a uniform high (potential) vorticity within the eye and zero vorticity outside. Vorticity waves propagate to the left of the vorticity gradient with respect to the mean cyclonic flow. Since the mean flow is strong the waves still move cyclonically, but with a much longer period. The predicted period is very close to the observed period. The fact that the linear theory predicts a smaller rotation period for the polygonal eyes also agrees qualitatively with the observations (Muramatsu 1986). The nonlinear theory stems from the rotation of the Kirchhoff vortex. With the observed ellipse radii, the Kirchhoff solution reduces to the linear wave period. The Rankine vortex structure is assumed in the theories and is shown to be important in the numerical experiments. The key point is that the basic flow in a Rankine vortex does support neutral wave solutions, which makes the elliptical eye rotation possible. On the other hand, a Rankine vortex structure for the minimum region in the center of the eye can distort the shape of the eye and change the rotation period due to the interaction of neutral vorticity waves. A fairly smooth (such as the Gaussian function) minimum vorticity region in the eye center does not distort the eye shape significantly. Estimations of eye rotation period from both linear and nonlinear theories seem to agree with the observation that an elliptical eye in a typhoon can rotate cyclonically with a period of approximately 144 min.

Our argument, however, does not answer the question of what causes the formation of an elliptical eye in Typhoon Herb. The role of diabatic heating due to moist convection has yet to be included in the theory. Moreover, the detailed potential vorticity structure in Typhoon Herb is needed, but this is not possible with the very limited observations. The potential vorticity field in a typhoon is determined by the complex interaction of diabatic, frictional, and advective processes. The frictional convergence and moist convection continually act to concentrate high potential vorticity in the eyewall region. Due to the nature of convection, the potential vorticity generated should be highly asymmetric. This process is opposed by the asymmetry-damping mechanism (Carr and Williams 1989). Furthermore, there is no latent heat release in the central region of the eye. Large values of potential vorticity within the eye then would not tend to occur unless they were transported in from the eyewall region. The process of potential vorticity inward mixing might then be related to the asymmetric eye contraction mechanism proposed by

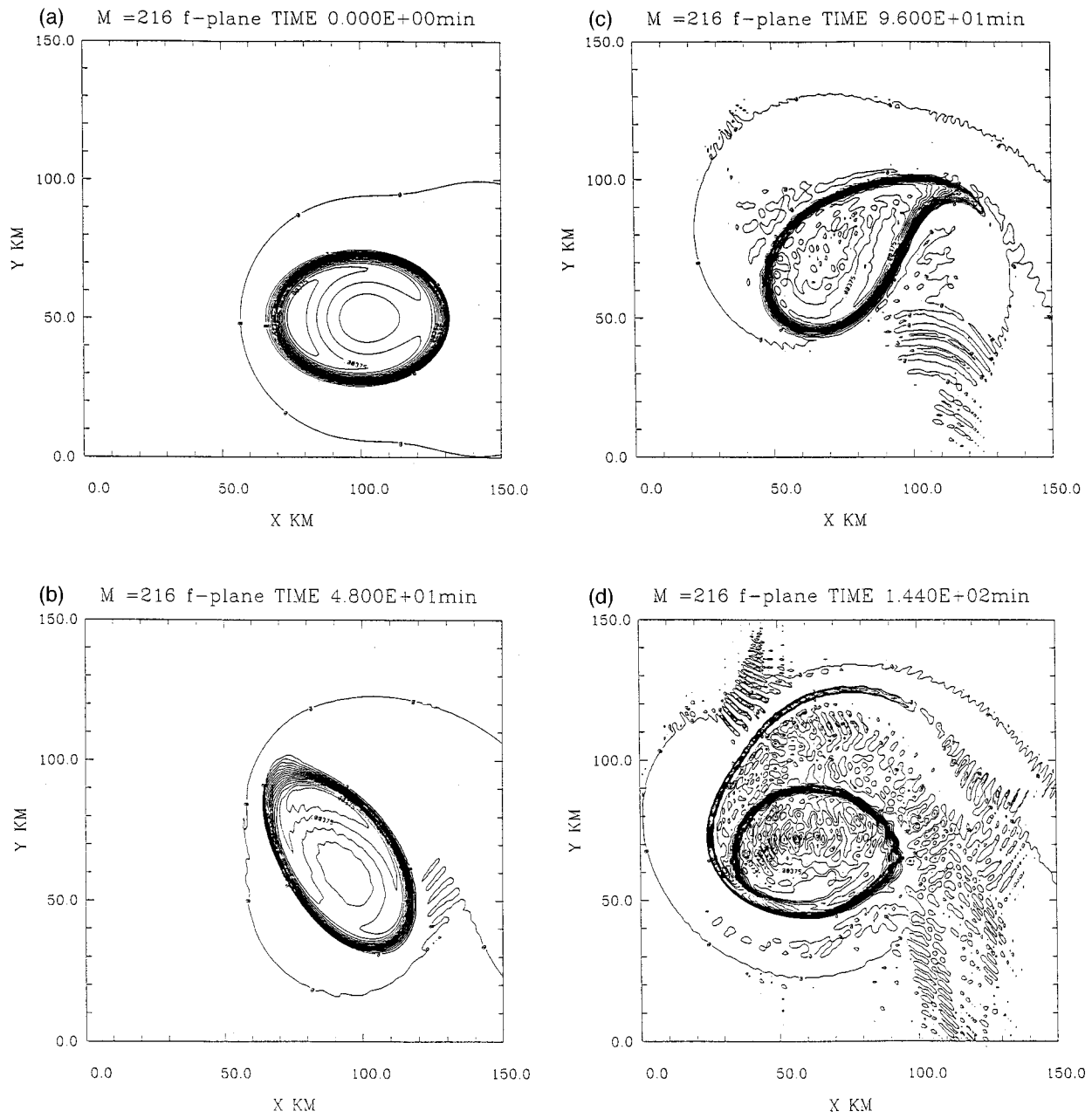

FIG. 9. The vorticity field for expt. 6 at 0, 48, 96, and 144 min. A neighboring vorticity field of 0.0015 s^{-1} is added outside the eye. A square region 150 × 150 km in the computational domain is shown. The contour interval is 0.00025 s^{-1}.

Schubert et al. (1997) and Schubert et al. (1999). To conserve angular momentum and/or kinetic energy during the redistribution process, the inward potential vorticity mixing must be accompanied also by some outward potential vorticity mixing. The outward mixing can be seen in the form of filaments that orbit the vortex core. Before we can fully understand the dynamics of eye rotation we need to know the timescale of the potential vorticity modification by moist physics, the timescale of potential vorticity axisymmetrization and redistribution, and the final resultant (potential) vorticity spatial structure. Because of the term $\boldsymbol{\zeta} \cdot \nabla\dot{\theta}$ in the potential vorticity equation, the potential vorticity modifications by diabatic heating are related to the relative spatial distribution of cumulus convection and vorticity within the tropical cyclone. In addition, the potential vorticity redistribution without an azimuthal wavenumber-one component can result in a very different macroscopic potential vorticity structure (Schubert et al. 1999). It is very likely that the adjustment timescales

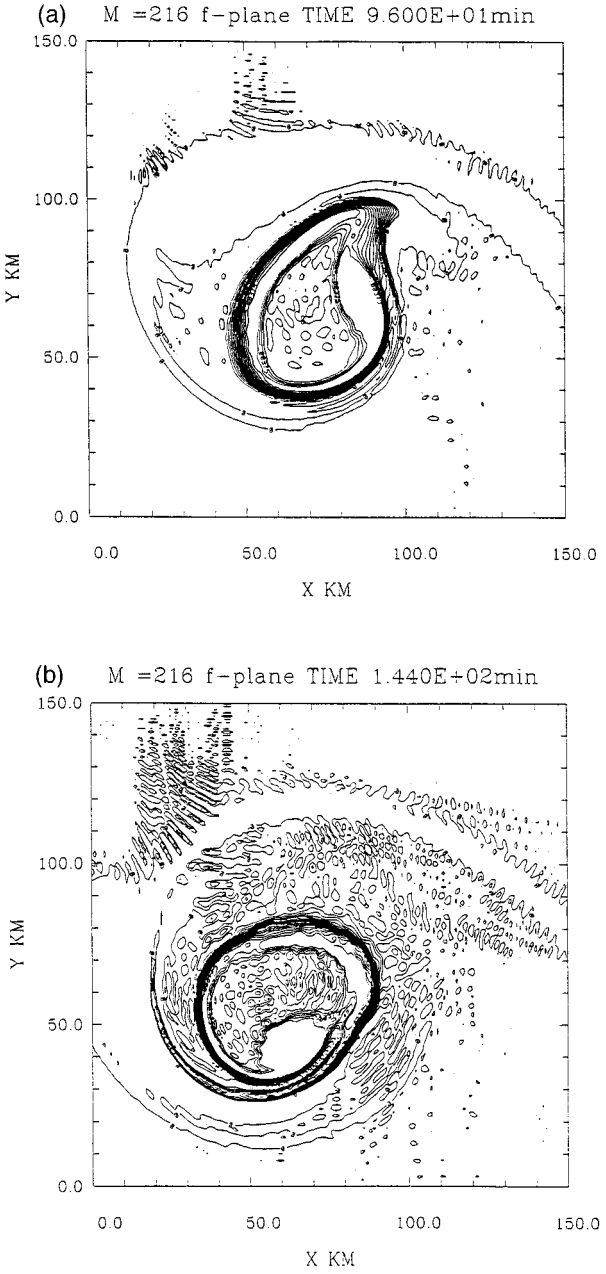

FIG. 10. The vorticity field for expt. 7 at 96 and 144 min. A neighboring vorticity field of 0.0015 s^{-1} is added outside the eye. A square region 150 × 150 km in the computational domain is shown. The contour interval is 0.00025 s^{-1}.

of potential vorticity by the redistribution and moist physics modification are initial condition dependent.

With simple dynamical model calculations, our intent is not to undermine the importance of the moist physics, but rather to isolate the fundamental dynamics believed responsible for the rotation of the elliptical eye in Typhoon Herb. There remains the question of how the (potential) vorticity is organized into the ''right'' structure and the ''right'' magnitude for our theory to be valid in a moist convective environment and in the presence of potential vorticity axisymmetrization and redistribution in a typhoon. This may be related to the important but unanswered question of eye dynamics. Without detailed observations of the potential vorticity distribution inside the eye region in Typhoon Herb, and without a thorough understanding of the eye dynamics, the question is difficult to answer. Simulations of Typhoon Herb by high-resolution ''full-physics models'' with a good physical initialization scheme and accurate cumulus parameterization may partially answer the question.

Acknowledgments. This research was supported by Grant NSC87-2111-M002-005 AP1 from the National Research Council of Taiwan, NSF Grant ATM-9525755, and P.E. 060435N from the Office of Naval Research through the Naval Research Laboratory. The authors would like to thank the Central Weather Bureau in Taiwan and Prof. Ben Jong-Dao Jou for providing the radar pictures. The authors would also like to thank Dr. L. E. Carr III for making available his derivation of the equations in the appendix for comparison. We also like to thank Drs. W. H. Schubert and M. T. Montgomery for useful comments in the paper.

APPENDIX

Vortex Stability with Three Constant Vorticity Regions

The original stability analysis for this problem was carried out by Michalke and Timme (1967). Our main goal is to determine the structure of the neutral waves. We begin with linearized nondivergent dynamics on a basic-state tangential flow that varies with radius

$$\left(\frac{\partial}{\partial t} + \frac{V}{r}\frac{\partial}{\partial \lambda}\right)\nabla^2\psi - \frac{1}{r}\frac{d\overline{\zeta}}{dr}\frac{\partial \psi}{\partial \lambda} = 0, \qquad \text{(A.1)}$$

where V and $\overline{\zeta}$ are the basic tangential wind and vorticity, respectively. The boundary conditions for (A.1) are $\psi \to 0$ at $r = 0$ and $r \to \infty$. The basic-state vorticity is assumed to have three constant vorticity regions. For the basic-state vorticity defined by

$$\overline{\zeta}(r) = \frac{d(rV)}{rdr} = \begin{cases} \zeta_0 - \Delta\zeta, & 0 < r < R_1, \\ \zeta_0, & R_1 < r < R_2, \\ 0, & R_2 < r < \infty, \end{cases} \qquad \text{(A.2)}$$

the corresponding basic-state tangential wind is

$$V = \frac{1}{2}\begin{cases} r(\zeta_0 - \Delta\zeta), & 0 \le r \le R_1, \\ r\zeta_0 - \dfrac{R_1^2}{r}\Delta\zeta, & R_1 \le r \le R_2, \\ \dfrac{R_2^2}{r}(\zeta_0 - \delta^2\Delta\zeta), & R_2 \le r \le \infty, \end{cases} \qquad \text{(A.3)}$$

where ζ_0, $\Delta\zeta$, R_1, and R_2 are constants and $\delta = (R_1/R_2)$.

The ζ_0 and $\Delta\zeta$ are the vorticity jumps at R_2 and R_1. The case in which we are interested has $\Delta\zeta > 0$ and $\zeta_0 > 0$, that is, a ring of elevated vorticity. From (A.3) we have

$$V_1 = V(R_1) = \frac{R_1}{2}(\zeta_0 - \Delta\zeta), \tag{A.4a}$$

$$V_2 = V(R_2) = \frac{R_2}{2}(\zeta_0 - \delta^2\Delta\zeta). \tag{A.4b}$$

Within each region $d\overline{\zeta}/dr = 0$, so a solution to the vorticity equation is zero disturbance vorticity everywhere except near the edge of the vorticity jumps. Searching for model solutions of the form $\psi = \Psi(r)e^{i(m\lambda-\sigma t)}$ to the vorticity equation, where m is the tangential wavenumber and σ the complex frequency, we obtain

$$\frac{d^2\Psi}{dr^2} + \frac{1}{r}\frac{d\Psi}{dr} - \frac{m^2}{r^2}\Psi = 0 \quad \text{for } r \neq R_1, R_2. \tag{A.5}$$

The two linearly independent solutions of (A.5) are $\Psi = r^m$ and $\Psi = r^{-m}$. The general solutions in the three regions that satisfy the limiting boundary conditions are

$$\Psi = \begin{cases} Ar^m, & 0 \le r \le R_1; \\ Br^m + Dr^{-m}, & R_1 \le r \le R_2; \\ Er^{-m}, & R_2 \le r \le \infty. \end{cases} \tag{A.6}$$

The solutions must be continuous at $r = R_1$ and $r = R_2$, which gives the conditions

$$A = B + DR_1^{-2m}, \tag{A.7a}$$

$$E = BR_2^{2m} + D. \tag{A.7b}$$

To relate Ψ at $r = R_1$ and $r = R_2$, we integrate (A.1) over the narrow intervals between $r = R_1 - \epsilon$ and $r = R_1 + \epsilon$ and between $r = R_2 - \epsilon$ and $r = R_2 + \epsilon$ with $\epsilon \to 0$ to obtain the jump conditions

$$\left(\frac{V_1}{R_1} - \frac{\sigma}{m}\right)\left[\left(\frac{d\Psi}{dr}\right)_+ - \left(\frac{d\Psi}{dr}\right)_-\right] - \frac{\Delta\zeta}{R_1}\Psi(R_1) = 0, \tag{A.8a}$$

and at $r = R_2$,

$$\left(\frac{V_2}{R_2} - \frac{\sigma}{m}\right)\left[\left(\frac{d\Psi}{dr}\right)_+ - \left(\frac{d\Psi}{dr}\right)_-\right] + \frac{\zeta_0}{R_2}\Psi(R_2) = 0. \tag{A.8b}$$

Now introducing the solution (A.6) into (A.8) gives

$$\left(\frac{V_1 m}{R_1} - \sigma\right)[m(BR_1^{m-1} - DR_1^{-m-1}) - mAR_1^{m-1}] - \frac{m}{R_1}\Delta\zeta AR_1^m = 0, \tag{A.9a}$$

$$\left(\frac{V_2 m}{R_2} - \sigma\right)[-mER_2^{-m-1} - m(BR_2^{m-1} - DR_2^{-m-1})] + \frac{m}{R_2}\zeta_0 ER_2^{-m} = 0. \tag{A.9b}$$

If we substitute A and E from (A.7) into (A.9), we have

$$\left(\frac{V_1 m}{R_1} - \sigma\right)(-2DR_1^{-2m}) - \Delta\zeta(B + DR_1^{-2m}) = 0, \tag{A.10a}$$

$$\left(\frac{V_2 m}{R_2} - \sigma\right)(-2BR_2^{2m}) + \zeta_0(BR_2^{2m} + D) = 0. \tag{A.10b}$$

Let $\sigma_1 = mV_1/R_1$ and $\sigma_2 = mV_2/R_2$ be the frequencies associated with the basic flows at R_1 and R_2, so that (A.10) can be written

$$-\Delta\zeta B - [2(\sigma_1 - \sigma) + \Delta\zeta]R_1^{-2m}D = 0, \tag{A11.a}$$

$$[-2(\sigma_2 - \sigma) + \zeta_0]R_2^{2m}B + \zeta_0 D = 0. \tag{A11.b}$$

For the nontrivial solutions for B and D we obtain

$$\sigma^2 - \left[\sigma_1 + \sigma_2 + \frac{1}{2}(\Delta\zeta - \zeta_0)\right]\sigma + \sigma_1\sigma_2 + \frac{1}{2}(\sigma_2\Delta\zeta - \sigma_1\zeta_0) - \frac{1}{4}\Delta\zeta\zeta_0(1 - \delta^{2m}) = 0. \tag{A.12}$$

The solution of (A.12) is

$$\sigma = \frac{\sigma_1 + \sigma_2}{2} + \frac{\Delta\zeta - \zeta_0}{4} \pm S^{1/2}, \tag{A.13}$$

where

$$S = \left(\frac{\sigma_2 - \sigma_1}{2} + \frac{\Delta\zeta + \zeta_0}{4}\right)^2 - \frac{\Delta\zeta\zeta_0}{4}\delta^{2m}. \tag{A.14}$$

Equation (A.14) shows that instability is only possible for $\Delta\zeta > 0$; that is, the basic-state vorticity jumps are of opposite sign. Moreover, one can verify from (A.14) that $S > 0$ for $m = 1$ and 2 despite the conditions $\Delta\zeta > 0$ and $\delta \neq 0$. This implies that the wavenumbers 1 and 2 are always stable. Equations (A.13) and (A.14) suggest the existence of two vorticity wave solutions that propagate along the interphases without the influence of the other interphase [these can be found by dropping the D term in (A.11b) and the B term in (A.11a) separately]. Finally, for either $\Delta\zeta = 0$ or $\delta \to 0$ one of the roots becomes the one jump solution

$$\sigma = \frac{\zeta_0}{2}(m - 1), \tag{A.15}$$

which is equivalent to (2.1a).

Using the parameters $\Delta\zeta = \frac{2}{3}\zeta_0$ and $\delta = \frac{1}{2}$ in experiment 3 and with $m = 2$, we have $[\sigma_-, \sigma_+] = \zeta_0[0.37, 0.63]$. Thus, we have one stable solution that is slower than the one jump solution ($\sigma = \zeta_0/2$) and another that is faster. The slower solution is slower than the one jump solution because the mean flow is slower (the mean vorticity is less). The faster solution is associated with the inner jump and the Rossby wave is reversed. The wavenumber 4 is stable in experiment 3. The frequencies associated with the wavenumber 4 are $[\sigma_-, \sigma_+] = \zeta_0[1.02, 1.15]$.

By using (A.7), we can evaluate the ratio of the streamfunction at $r = R_1$ to the value at $r = R_2$:

$$\frac{\Psi(R_1)}{\Psi(R_2)} = \frac{R_1^m A}{R_2^{-m} E} + \frac{R_1^m B + DR_1^{-m}}{R_2^m B + DR_2^{-m}}.$$

This ratio can be written in terms of the frequency with either (A.11a) or (A.11b). For example, the ratio from (A.11a) is

$$\frac{\Psi(R_1)}{\Psi(R_2)} = \delta^{-m} \frac{2(\sigma_1 - \sigma)}{2(\sigma_1 - \sigma)\delta^{-2m} + \Delta\zeta(1 - \delta^{-2m})}. \quad \text{(A.16)}$$

This equation can be evaluated with either σ_+ or σ_- to find the relative importance of the solutions at the two radii. For experiment 3 and $m = 2$, the ratios are

$$\frac{\Psi(R_1)}{\Psi(R_2)} \sim -5$$

for $\sigma_+ = 0.63\zeta_0$ and

$$\frac{\Psi(R_1)}{\Psi(R_2)} \sim -\frac{1}{30}$$

for $\sigma_- = 0.37\zeta_0$. This indicates that the slow solution is about 30 times larger at R_2 than at R_1, while the faster solution is 5 times larger at R_1 than at R_2. Also, the solutions are out of phase at the two radii.

REFERENCES

Carr, L. E., III, and R. T. Williams, 1989: Barotropic vortex stability to perturbations from axisymmetry. *J. Atmos. Sci.,* **46,** 3177–3191.

Dritschel, D. G., 1998: On the persistence of non-axisymmetric vortices in inviscid two-dimensional flows. *J. Fluid Mech.,* **371,** 141–155.

Fulton, S. R., and W. H. Schubert, 1987: Chebyshev spectral methods for limited-area models. Part I: Model problem analysis. *Mon. Wea. Rev.,* **115,** 1940–1953.

Guinn, T., and W. Schubert, 1993: Hurricane spiral bands. *J. Atmos. Sci.,* **50,** 3380–3404.

Kuo, H.-C., and W. H. Schubert, 1988: Stability of cloud-topped boundary layers. *Quart. J. Roy. Meteor. Soc.,* **114,** 887–916.

Kurihara, Y., 1976: On the development of spiral bands in a tropical cyclone. *J. Atmos. Sci.,* **33,** 940–958.

——, and M. A. Bender, 1982: Structure and analysis of the eye of a numerically simulated tropical cyclone. *J. Meteor. Soc. Japan,* **60,** 381–395.

Lamb, H., 1932: *Hydrodynamics.* 6th ed. Dover, 732 pp.

Lee, W. C., 1997: Structure of Typhoon Herb (1996) observed by WSR-88D in Taiwan. Preprints, *22d Conf. on Hurricanes and Tropical Meteorology,* Ft. Collins, CO, Amer. Meteor. Soc., 670–671.

Lewis, B. M., and H. F. Hawkins, 1982: Polygonal eye walls and rainbands in hurricanes. *Bull. Amer. Meteor. Soc.,* **63,** 1294–1300.

Melander, M. V., J. C. McWilliams, and N. J. Zabusky, 1987: Axisymmetrization and vorticity-gradient intensification of an isolated two-dimensional vortex through filamentation. *J. Fluid Mech.,* **178,** 137–159.

Michalke, A., and A. Timme, 1967: On the inviscid instability of certain two-dimensional vortex-type flows. *J. Fluid Mech.,* **29,** 647–666.

Montgomery, M. T., and R. J. Kallenbach, 1997: A theory for vortex Rossby-waves and its application to spiral bands and intensity changes in hurricanes. *Quart. J. Roy. Meteor. Soc.,* **123,** 435–465.

——, and J. Enagonio, 1998: Tropical cyclogenesis via convectively forced vortex Rossby waves in a three-dimensional quasigeostrophic model. *J. Atmos. Sci.,* **55,** 3176–3207.

Muramatsu, T., 1986: The structure of polygonal eye of a typhoon. *J. Meteor. Soc. Japan,* **64,** 913–921.

Schubert, W. H., M. T. Montgomery, R. K. Taft, T. A. Guinn, S. R. Fulton, and J. P. Edwards, 1997: Potential vorticity redistribution, asymmetric eye contraction and polygonal eyewalls in hurricanes. Preprints, *22d Conf. on Hurricanes and Tropical Meteorology,* Ft. Collins, CO, Amer. Meteor. Soc., 98–99.

——, ——, ——, ——, ——, J. P. Kossin, and J. P. Edwards, 1999: Polygonal eyewalls, asymmetric eye contraction, and potential vorticity mixing in hurricanes. *J. Atmos. Sci.,* **56,** 1197–1223.

Smith, G. B., and M. T. Montgomery, 1995: Vortex axisymmetrization: Dependence on azimuthal wavenumber or asymmetric radial structure changes. *Quart. J. Roy. Meteor. Soc.,* **121,** 1615–1650.

Thomson, W., 1880: Vibrations of a columnar vortex. *Phil. Mag.,* **10,** 155–168.

Willoughby, H. E., 1978: A possible mechanism for the formation of hurricane rainbands. *J. Atmos. Sci.,* **35,** 836–848.